The Major Stratospheric Sudden Warming of January 2013: Analyses and Forecasts in the GEOS-5 Data Assimilation System

LAWRENCE COY *

Global Modeling and Assimilation Office, NASA Goddard Space Flight Center, Greenbelt, MD

Science Systems and Applications, Inc., Lanham, MD

STEVEN PAWSON

Global Modeling and Assimilation Office, NASA Goddard Space Flight Center, Greenbelt, MD

* *Corresponding author address:* Lawrence Coy, Science Systems and Applications, Inc., 10210 Greenbelt Rd., Lanham, MD 20706.

E-mail: lawrence.coy@nasa.gov

ABSTRACT

We examine the major stratosphere sudden warming (SSW) that occurred on 6 January 2013, using output from the NASA Global Modeling and Assimilation Office (GMAO) GEOS-5 (Goddard Earth Observing System) near-real-time data assimilation system (DAS). Results show that the major SSW of January 2013 falls into the vortex splitting type of SSW, with the initial planetary wave breaking occurring near 10 hPa. The vertical flux of wave activity at the tropopause responsible for the SSW occurred mainly in the Pacific Hemisphere, including the a pulse associated with the preconditioning of the polar vortex by wave 1 identified on $\sim$23 December 2012. While most of the vertical wave activity flux was in the Pacific Hemisphere, a rapidly developing tropospheric weather system over the North Atlantic on $\sim$28 December is shown to have produced a strong transient upward wave activity flux into the lower stratosphere coinciding with the peak of the SSW event. In addition, the GEOS-5 5-day forecasts accurately predicted the major SSW of January 2013 as well as the upper tropospheric disturbances responsible for the warming. The overall success of the 5-day forecasts provides motivation to produce regular 10-day forecasts with GEOS-5, to better support studies of stratosphere-troposphere interaction.

1. Introduction

Modern global numerical weather prediction (NWP) systems are capable of providing accurate five-day forecasts and analyses of stratospheric circulations, including stratospheric sudden warming (SSW) events at state-of-the-art horizontal and vertical resolutions (Dörnbrack et al. 2012). Stratospheric forecasts are of interest because of the stratosphere's role as an upper boundary to the tropospheric weather forecasts and possible influence on global modes, such as the Arctic Oscillation (Baldwin and Dunkerton 2001) and Pacific blocking (Kodera et al. 2013). Stratospheric forecasts are especially intriguing as the stratosphere (with dynamics dominated by global scale vorticity advection) tends to be more predictable than the troposphere (Hoppel et al. 2008) so that, if the stratosphere has a significant influence on global modes, a realistic stratosphere may enhance their predictability. Stratospheric and tropospheric analyses are useful for dynamical studies of coupling between the troposphere and stratosphere, including the forcing of the stratospheric planetary waves by the troposphere and their subsequent vertical propagation and breaking (e.g., Harada et al. 2010). In addition, the higher horizontal resolution typically found in NWP systems allows for studies of resolved gravity wave coupling between the tropospheric and stratosphere.

Past studies have examined individual SSW events (e.g., Kuttippurath and Nikulin 2012; Harada et al. 2010; Coy et al. 2009) as well as composites of SSW events (e.g., Sjoberg and Birner 2012; Limpasuvan et al. 2004; Charlton and Polvani 2007). SSW events are characterized by enhanced planetary wave forcing by upper tropospheric weather disturbances and blocking ridges that act to generate planetary waves that propagate into the stratosphere. These upward propagating waves increase in amplitude (as density decreases) and interact strongly with the background flow creating the potential for "wave breaking", an irreversible mixing of Ertel potential vorticity (EPV) between low and high latitudes (McIntyre and Palmer 1983). If the planetary waves advect sufficient low EPV air poleward, the conservation of EPV will create a strong enough anti-cyclonic circulation in that air mass to displace or split the climatological cyclonic wintertime polar vortex. The warming results from the strong descent in the polar regions needed to balance the dynamical changes. These dynamical changes inhibit the further upward propagation of planetary waves causing them to break at lower levels than the initial wave breaking and hence result in the descending pattern of wind and temperature changes characteristic of a SSW event (Matsuno 1971). A major SSW occurs when the 10 hPa 60°N zonal mean zonal wind reverses from westerly to easterly and the 10 hPa zonal mean temperature gradient increases poleward of 60°N. If only the temperature gradient increases while the winds remain westerly then the SSW is considered minor (see Andrews et al. 1987, page 259). The composite studies of SSW evolution highlight the preconditioning of the polar vortex with strong planetary-wave-1 activity before the SSW, especially prior to the split vortex SSW events (Charlton and Polvani 2007). Recent studies of specific SSW events have focused on identifying tropospheric weather features such the large upper tropospheric ridge over the west coast of the US preceding the SSW of January 2009 (Harada et al. 2010) and the more transient ridge over the North Atlantic associated with the SSW of January 2006 (Coy et al. 2009). The analysis presented here will continue this focus of investigating the tropospheric structures preceding the SSW.

In this paper we examine the major stratosphere sudden warming (SSW) that occurred on 6 January 2013, as seen in the NASA Global Modeling and Assimilation Office (GMAO) GEOS-5 (Goddard Earth Observing System) near-real-time data assimilation system (DAS). We characterized the evolution of the SSW and the tropospheric weather systems that preceded the SSW event. We also evaluate the ability of the near-real-time five-day forecasts to predict the warming. In addition, while the zonal mean zonal wind reversal associated with a SSW can sometimes begin high in the mesosphere (Coy et al. 2011), the planetary waves initially break on a restricted altitude range in the middle stratosphere (e.g. Coy et al. 2009). We investigate the altitude of the initial wave breaking and relate this altitude to the downward propagation of the SSW wind and temperatures changes.

The plan of this paper is as follows: Section 2 gives a brief description of the GEOS-

5 DAS, Section 3 presents the results in terms of a overview of the January 2013 SSW, an examination of the three dimensional wave activity flux, and description of the upper tropospheric flow both before and during the SSW, and Section 4 provides a discussion and summary.

2. Data Assimilation System Description

For this study the near-real-time GMAO GEOS-5.7.2 system was used. The GEOS-5.7.2 system is updated from the version of GEOS-5 used in the MERRA (Modern-Era Retrospective Analysis for Research and Applications) project, which is described in detail in Rienecker et al. (2011, 2008) and Molod et al. (2012). One of the main differences between MERRA and the GEOS-5.7.2 system is the increased horizontal resolution used in the near-real-time system — a 0.3125° x 0.25° lon-lat grid was used. The analysis increments are calculated on a 0.625° x 0.5° lon-lat horizontal grid that are then interpolated onto the higher (0.25°) resolution as part of the assimilation cycle. The radiative transfer package and the model layers remain unchanged from MERRA.

The GEOS-5 DAS forecast model is based on a finite volume dynamical core (Lin 2004). Relevant physics for stratospheric studies include orographic (McFarlane 1987) and non-orographic (Garcia and Boville 1994) gravity wave drag, and short (Chou and Suarez 1999) and long wave (Chou et al. 2001) radiative transfer models valid up to $\sim$80 km. The three-dimensional variational analysis is done every six hours using the GMAO implementation of the GSI (Grid-point Statistical Interpolation) scheme (Wu et al. 2002; Purser et al. 2003a,b). Observational data include both conventional (radiosondes, aircraft, etc.) and available satellite radiances, with the AMSU-A (Advanced Microwave Sounding Unit) radiance channels 11–14 providing a major constraint in the stratosphere. An Incremental Analysis Update (IAU, Bloom et al. 1996) procedure gradually adds the analysis to the model as a dynamical forcing. The final three-dimensional output fields (winds and temperature) are saved every three hours. The GEOS-5 DAS has been successfully used for many studies including driving chemistry transport models (e.g. Pawson et al. 2007) and observation impact experiments (e.g. Gelaro et al. 2010).

3. Results

a. SSW Overview

This section examines the time evolution of the 2013 major SSW. Figure 1 shows an overview of 10 hPa wind, temperature, and planetary waves 1–3 during the SSW, as analysed in GEOS-5 for 11 December 2012 through 10 February 2013, along with GEOS-5 daily 5-day forecast output.

The 10 hPa temperature at the North Pole (Fig. 1a) is 200 K on 1 January 12 UTC increasing up to 240 K by 6 January 12 UTC for a 40 K change in 5 days. After the rapid rise, the polar temperature remains warm until ∼18 January, followed by a slower decay back to near 200 K by 10 February. The 12 UTC 5-day forecasts of 10 hPa polar temperature closely follow the analysis temperatures during this time period, including the rapid rise in polar temperature characteristic of the major SSW.

The 60°N zonal mean of the zonal wind (Fig. 1b) decreases as the 10 hPa polar temperature increases, changing from westerly to easterly on 6 January 12 UTC. Coupled with the reversed 60°N to pole 10 hPa temperature gradient (Fig. 2a) this change in sign of the 10 hPa zonal mean zonal wind determines the time of the SSW event, 6 January 12 UTC 2013. These winds, after coming close to zero on 10 January, remain easterly until 28 January. The forecasted values of the 10 hPa, 60N, zonal mean zonal wind tracks the analysis, closely following the westerly wind decrease and the change to easterly winds associated with the SSW.

The evolution of the 10 hPa 60°N meridional wind amplitude of zonal waves 1–3 during the major SSW is shown in Fig. 1c. Wave 1 dominates over waves 2 and 3 prior to the

SSW with a varying amplitude near $\sim$25 ms^{-1}. This wave 1 amplitude rapidly decreases to $\sim$10 ms^{-1} or less during the SSW and remains relatively low thereafter. The wave 2 amplitude increases before the SSW, however it is still less than 20 ms^{-1} on 4 January 12 UTC. During the SSW the wave-2 amplitude increases rapidly up to 38 ms^{-1} on 8 January 12 UTC, nearly doubling in amplitude over 4 days. Following the SSW, the wave 2 meridional wind amplitude continues being large ($<$ 20 ms^{-1}) out to 15 January, after that time it decays, becoming less than $\sim$10 ms^{-1} on 22 January. The wave 3 amplitude peaks on the date of the SSW wind reversal (6 January) and is relatively small at other times, though it is smaller after the SSW than before. The 5-day forecast of the 10 hPa 60°N meridional wind wave 1–3 amplitude (plus symbols) shows fair agreement with the analysis amplitudes. Note that, through geostrophy, the meridional wind is closely related to the longitudional gradient of the geopotential height field, $v_{geo} \propto k\Phi$, where k is the zonal wavenumber, and therefore the meridional wind wave amplitudes (while not strictly geostrophic in the data assimilation system) will emphasize the higher wavenumbers more than a similar examination of geopotential height wave amplitudes would. Because meridional wind is an important dynamical component during SSW vortex breakup, meridional wind wave amplitudes are plotted in Fig. 1c rather than the more traditional geopotential height wave amplitudes.

The ability of the GEOS-5 data assimilation system to forecast the dramatic circulation changes in 10 hPa zonal averaged temperature and zonal wind characteristic of SSW events is shown in Fig. 2. On 2 January 2013 12 UTC, the zonal average analysis temperature is over 20 K cooler at 90°N compared with 60°N (Fig. 2a, red curve) while the 5-day forecast (blue curve) has reversed this zonal mean temperature gradient with the polar temperature on 7 January predicted to be over 15 K warmer than the 60°N temperature. The 10 hPa zonal averaged zonal wind 5-day forecast (Fig. 2b, blue curve) shows a change of $\sim$65 ms^{-1} from westerly to easterly winds when compared to the initial 2 January analysis winds (red curve). The temperature and wind verifying analyses on 7 January 12 UTC (green curves) show good agreement with the predicted 5-day changes. This forecast of the January 2013 major SSW was identified on 3 January 2013 as part of the routine monitoring of the GEOS-5 system.

A synoptic overview of the middle stratosphere vortex breakdown during the SSW is shown at four times (5-day intervals) in Fig. 3, with Figs. 3b and 3c corresponding to the analyses associated with the initial and final times (2 January and 7 January) of the 5-day forecast results shown in Fig. 2. The Ertel Potential Vorticity (EPV) fields on the 840 K potential temperature surface ($\sim$10 hPa) show the polar vortex (high EPV values) displaced off the pole in a mainly wave 1 pattern (Fig. 3a, 28 December) followed by the advection of low EPV air from low latitudes ($< 30°$N) toward 180°E (Fig. 3b, 2 January), the development of a substantial low EPV region near 180°E and the near splitting of the polar vortex (Fig. 3c, 7 January), and the vortex fully split (Fig. 3d, 12 January). The 10 hPa geopotential height fields, also shown in Fig. 3, closely follow the 840 K EPV fields, outlining the regions of high and low EPV. The overall synoptic pattern shows the vortex displaced off the pole followed by a splitting of the displaced vortex.

The zonally averaged forcing of the SSW from the troposphere can be characterized by an examination of the upward Eliassen-Palm (EP) flux (see Andrews et al. 1987, page 128) near the tropopause ($\sim$100 hPa). Figure 4 shows the upward EP flux at 100 hPa from 1 December 2012 to 31 March 2013, as a function of time and latitude, and broken down in terns of zonal waves 1 and 2. The total upward EP flux (Fig. 4a) shows relatively high values from the end of December through the beginning of February before dropping off in the rest of February and March. Note the high latitude peaks near 23 December and 6 January that were associated with the preconditioning of the polar vortex and the middle of the SSW, respectively. The wave 1 contribution (Fig. 4b) occurs mainly before the SSW, while the wave 2 contribution (Fig. 4c) occurs mainly during and after the SSW. The time series of the 30°–90°N averages of the upward EP fluxes are shown in Fig. 4d for comparison with similar figures in Harada et al. (2010) for the Northern Hemisphere winters of 1984/85, 1988/89, and 2008/09. The latitudinally averaged wave 1 upward EP flux (red curve) decreases during the SSW as the wave 2 EP flux (blue curve) increases. The wave 3 forcing (green curve) increases somewhat during the SSW but remains relatively small. The wave 2 EP flux maxima found before and during the SSW are less than one ($\times 10^5$ Kg s^{-2}), smaller than the maximum values found during any of the three winters examined by Harada et al. (2010). Thus, the major vortex-splitting SSW of 2013 had a relatively weak forcing contribution from the wave 2 component of the vertical EP flux.

b. *Wave Activity Flux*

Up to this point, we have focused on the SSW evolution in the middle stratosphere (10 hPa) and the zonally averaged EP flux forcing near the tropopause ($\sim$100 hPa). To better understand the vertical and horizontal dependence of the SSW evolution we have calculated the three-dimensional wave activity flux developed by Plumb (1985):

$$\mathbf{F}_s = p\cos\phi \begin{pmatrix} v'^2 - \frac{1}{2\Omega a \sin 2\phi}\frac{\partial(v'\Phi')}{\partial\lambda} \\ -u'v' - +\frac{1}{2\Omega a \sin 2\phi}\frac{\partial(u'\Phi')}{\partial\lambda} \\ \frac{2\Omega\sin\phi}{S}[v'T' - \frac{1}{2\Omega a \sin 2\phi}\frac{\partial(T'\Phi')}{\partial\lambda}] \end{pmatrix}, \tag{1}$$

where p is normalized pressure (1 at the surface), u and v are the zonal and meridional wind components respectively, T is temperature, Φ is geopotential height, λ and ϕ are longitude and latitude respectively, a is the Earth's radius, Ω is the frequency of the Earth's rotation, and S is a measure of average static stability (taken to be constant here). This wave activity flux formulation was used by Harada et al. (2010) in their study of the major SSW of January 2009. When Eq. 1 is zonally averaged the meridional and zonal components reduce to the corresponding components of the quasi-geostropic Eliassen-Palm flux (Andrews et al. 1987). Here we investigate some aspects of the vertical/horizontal evolution of the major SSW of January 2013 based on averages of zonal wind and wave activity flux over limited longitudinal ranges.

To examine in more detail the development of the 10 hPa high pressure, low EPV region, near 180°E longitude seen in Fig. 3, the zonal wind and wave activity flux are averaged over hemispheric domains centered on 0°E and 180°E (hereafter referred to as the Atlantic and Pacific hemispheres, respectively) and plotted as latitude verses altitude cross sections (Fig. 5). The anticyclone initially develops at ∼10 hPa altitude, 40°-50°N (Figs. 5a and b, 28 and 30 December) as can be seen in the growing easterly (shaded) and westerly wind couplet in the Pacific hemisphere (left side of the panels in Fig. 5). This anticyclone strengthens considerably by 1 January (Fig. 5c), as seen by the stronger winds in the Pacific hemisphere between 10–1 hPa, and the vertical tilt of the anticyclone has moved slightly poleward at this time. By 3 January (Fig. 5d) the anticyclone has continued to increase in strength, has moved poleward to ∼60°N, and now extends above 1 hPa into the mesosphere as well as down into the lower stratosphere. By 5 January (Fig. 5e) the anticyclone continues to move poleward, especially in the mesosphere, producing strong winds across the pole and by 7 January (Fig. 5d) the anticyclone is nearly over the pole as the vortex splits at this time. In the Atlantic hemisphere (0°E, right side of panels in Fig. 5) the westerlies (shaded) gradually decrease in strength and shift equatorward, especially from 3–5 January (Figs. 5d and e).

The wave activity flux vectors (Fig. 5) are generally larger in the Pacific than the Atlantic hemisphere. Strong poleward focusing of the vectors is found on 5 January (Fig. 5e) in the lower stratosphere, Pacific hemisphere, when the anticyclone moves over the pole. This identifies most of the poleward focusing in the zonally averaged EP flux as being located in the Pacific hemisphere. Note that, from Eq. 1, the wave activity vectors tend to zero toward the pole, as the wave perturbations are defined with respect to a zonal average, so it is not possible to follow wave propagation across the pole in this formulation. Also on 5 January the Pacific wave activity flux extends to the Equator in the lower mesosphere (∼0.5 hPa), just below the semiannual westerlies, indicating wave propagation into the equatorial region. On 7 January (Fig. 5d) the Pacific hemisphere wave activity flux vectors remain large, extending well into the mesosphere, denoting strong wave propagation continuing in this hemisphere at this time. The wave activity vectors in the Atlantic hemisphere are largest on

3–5 January (Figs. 5d and e), the time when the vortex is moving away from the pole. Note that the arrows have been scaled in the vertical so that they no longer visually illustrate the divergence, however they show the relative amplitudes at each pressure level as a function of latitude and the six times shown.

c. Upper Troposphere Synoptic Systems

In this section we examine some of the upper tropospheric systems that occurred before and during the January 2013 SSW event. These include high latitude, ridge events over the Pacific Hemisphere prior to the SSW (24 December) and over the Atlantic Hemisphere during the SSW event (6 January). A rapidly developing tropospheric system over the North Atlantic will be examined in the following subsection.

In Figs. 6, 7, and 8 the relation between the troposphere jet at 300 hPa and the lower stratosphere vortex (50 hPa geopotential heights) is explored. The tropospheric ridge responsible for the relatively early (24 December) vertical wave activity flux at high latitudes initially formed near 180°E on 20 December (Fig. 6a), moved eastward, increased in meridional amplitude (Fig. 6b), extended under the lower stratospheric jet (Fig. 6c), and formed a high latitude cut-off high that reached the pole by 23 December. The lower latitude (40°–60°N) vertical wave activity flux (not shown) peaked on the west side of the ridge on 21 December. The upper tropospheric ridge remained strong on 24 December (Fig. 7a), however, by 25 December (Fig. 7b), it had decayed substantally as the large-scale, lower stratospheric ridge above (at 50 hPa) the upper tropospheric ridge continued to increase in amplitude. Though the upper tropospheric flow on 26–27 December (Figs. 7c and d) undulated without a major ridge over the US and the eastern Pacific, the lower stratosphere high persisted in that region. In summary, there is an upper tropospheric cut-off high associated with the development of a large ridge in the lower stratosphere.

The development of the upper tropospheric and lower stratosphere circulation during the warming is shown in Fig. 8. On 3 January (Fig. 8a) the lower stratospheric ridge over the US has decayed and the lower stratospheric vortex shows a wave-3 shape combined with non-zero wave 1 and 2 components. Upper tropospheric ridges are prominent over the western US and over the North Atlantic on 3 January, however only the ridge over the North Atlantic strengthens (Fig. 8b), extending under the stratospheric vortex by 5 January (Fig. 8c) and persisting through 6 January (Fig. 8d), a time when the lower stratospheric vortex begins to split as part of the SSW with strong 50 hPa ridges over both the Eastern Pacific and the North Atlantic.

Accurate forecasting of upper tropospheric ridge development is likely important in forecasting the SSW events. Figure 9 shows the GEOS-5 5-day forecasts for the same times and quantities as plotted in Fig. 8. The overall agreement between the 5-day forecasts and the analyses are good. Specifically, development of the upper tropospheric ridge near 0°E to high latitudes is captured by the 5-day forecast. The poorest agreement occurs on 3 January (Fig. 9a) where the two upper tropospheric ridges in the forecasts have less eastward tilt with latitude than those in the analysis. This corresponds to less horizontal heat flux and hence an underestimate of vertical wave propagation in the forecasts.

While the high-latitude wave forcing reveals the patterns associated with the high-latitude upper tropospheric ridge development, most of the vertical wave forcing occurs at middle latitudes. Figure 10 shows the vertical component of the wave activity flux averaged over 30°–60°N for the two hemisphere examined above over the 16 December 2012 to 20 January 2013 period. The vertical propagation near the tropopause is larger in the Pacific hemisphere (Fig. 10a) than in the Atlantic hemisphere (Fig. 10b). There are three main forcing events identifiable, with 100 hPa peak values on 23 December, 3 January, and 14 January. Note that there is a consistent time-lag of $\sim$4 days between the upward flux maxima in the mid-troposphere and the delayed upward flux maxima at 100 hPa. At these latitudes there is no evidence of an upward flux peak on 6 January associated with the high-latitude ridge seen at that time. Before 23 December the upward wave activity flux at 100 hPa is weak. The 23 December upward flux event is evident in both hemispheres but stronger in the Pacific hemisphere. Moreover, the upward flux at this time propagates vertically more rapidly in the Atlantic hemisphere than in the Pacific hemisphere, as shown by the black arrows. The strong upward wave activity flux across the tropopause on 3 January only occurs in the Pacific hemisphere, implying that wave 2 forcing at these latitudes is not especially large at this time. The upward wave activity flux after the SSW on 13 January is once again largest in the Pacific hemisphere and shows that the lower stratosphere still supports significant wave activity at this time. Another feature of the Pacific hemisphere that is missing in the Atlantic hemisphere is the strong upward flux in the upper stratosphere and lower mesosphere the occurs on ~9 January after SSW has satisfied the major warming criteria.

Figure 11 summarizes the upward wave activity flux at 100 hPa, averaged over 30°–90°N and presented as a function of time and longitude. The regions of strong upward wave activity flux (red shaded contours) are generally located in the Pacific hemisphere before and during the SSW, with the exception of a small region near 0°E on ~23 January and a weak (yellow shaded contours) region near 30°W on ~1–10 January. While these exceptions make a wave 2 contribution to the SSW forcing, the main upward wave activity flux is confined to the Pacific hemisphere, and is thus predominately a wave 1 signal.

d. Tropospheric storm of 29 December 2013

Prior to the major SSW a low surface pressure system rapidly developed at high latitudes near 0°E longitude (Fig. 12). The GEOS-5 analysis surface pressure at the center of the low decreased by more than 24 hPa in 24 hrs from 28 to 29 December 2013 (973 to 940) reaching the '"bomb" definition at this time (Sanders and Gyakum 1980). This surface development occurs under the strong lower stratospheric vortex winds, identified by the strong gradient in the 50 hPa geopotential heights. This section examines the development of the 29 December storm as related to the associated lower stratospheric changes.

In Coy et al. (2009) synoptic scale disturbances in the upper troposphere, characterized by large fluctuations in the 360 K potential temperature surface, were shown to precede the major SSW events of January 2003 and January 2006. The 360 K surface typically varies from ∼9–18 km in December–January, closely mirroring upper tropospheric (200 hPa) temperatures with cold (warm) temperatures corresponding to high (low) 360 K heights. To the extent that the potential temperature surface resembles a material surface its height fluctuations will influence the atmosphere above. As noted in Coy et al. (2009), high 360 K potential temperature surface heights also coincide with low column ozone values, reinforcing the idea that these are regions where strong vertical uplift has occurred.

Figure 13 shows snapshots of the upper tropospheric 360 K surface deviations from a 7 day running average superimposed with the lower stratospheric 50 hPa surface on 27–30 December 2012. Subtracting the 7 day time average removes the persistently high tropical and polar heights revealing the mid-latitude, synoptic variations. From 27-28 December (Figs. 13a and b) the weather systems over the North Atlantic are propagating to the north east, moving under the strong polar vortex winds, and increasing in amplitude. As the surface pressure decreases on 29 December, the high 360 K heights increase slightly, tracking under the stratospheric vortex winds (Fig. 13c). By 30 December the high and low 360 K perturbations decrease in amplitude (Fig. 13d). Note that there is also a high 360 K surface increasing in amplitude near 140°E at the outer edge of the stratospheric polar vortex.

An overview of the 360 K potential temperature heights during 15 December 2012 to 15 January 2013 is shown in Fig. 14 where the height perturbations are averaged from 45°-75°N and plotted as a function of longitude and time. The amplitude of the North Atlantic storm in the upper troposphere stands out as the largest upper tropospheric event over this time period at these latitudes.

A longitude pressure cross section through the storm at 60°N on 29 December (Fig. 15) shows an increase in 24 hr geopotential height change near 0°E in the upper troposphere. Lower stratospheric height changes are concentrated from 60°W–90°E, above the tropospheric changes. The 24 hr change in wave activity flux (arrows) shows upward wave influence increasing ahead of the developing tropospheric high. The potential temperature surfaces show a longitudinal gradient region in the stratosphere near 0°E associated with the polar vortex. The tropospheric storm is developing under this gradient region.

If this tropospheric system is important in forcing the SSW, then realistically forecasting this system becomes important in forecasting the SSW. Figure 16 plots the same fields as in Fig. 15 for the corresponding 5-day forecast. The 5-day forecast picks up the main features seen in the analysis, including the increasing tropospheric high, the increasing perturbations in the lower stratosphere above the tropospheric high, the increasing vertical wave activity flux and the perturbations in the 360 K potential temperature surface. The forecasted 24 hr changes generally have larger amplitudes than those seen in the analysis.

Figure 17 shows the standard deviation of the 360 K potential temperature surface and the 50 hPa geopotential heights averaged over 3 days during the development of the troposphere North Atlantic storm prior to the SSW and for 3 days after the SSW event. Regions where these standard deviations are large denote strong upper tropospheric storm tracks. Before the SSW (Fig. 17a) the upper tropospheric storm track is strong over the North Atlantic and Northern Europe, under the 50 hPa height gradient. There is also a region near 155°E that is under the equatorial side of the 50 hPa height gradients (the vortex edge) and similarly a small region near 70°E. A strong storm track is also locate over the southeastern U.S., however this region is far south of the polar vortex. After the SSW the North Atlantic storm track is gone and the strongest deviations are found over the Pacific. The strong storm tracks seen under the stratospheric vortex prior to the SSW likely play a role in forcing the stratospheric wave development responsible for the SSW.

4. Discussion and Summary

The evolution of the 10 hPa geopotential height field (Fig. 3) shows that the major SSW of January 2013 falls into the vortex splitting type SSW, which is distinct from a vortex displacement type SSW (Charlton and Polvani 2007). The SSW became a major

SSW on 6 January 2013 when the 10 hPa 60°N zonal mean zonal wind reversed direction from westerly to easterly, accompanied by a change in the zonal mean, 60°–90°N, 10 hPa temperature gradient from negative to positive at that time, satisfying the criteria for a major SSW (Figs. 1 and 2).

The wave breaking and concomitant increase in poleward advection of low EPV associated with the major SSW occurs first near 10 hPa, increasing the amplitude of the climatological Aleutian high (Harvey and Hitchman 1996) in the Pacific hemisphere (Fig. 5). The wave activity flux is also greatest in this hemisphere over the course of the SSW event. The tilt of the upward developing high towards the pole, consistent with Aleutian high climatology of Harvey and Hitchman (1996), causes the SSW changes to first appear at somewhat higher levels near the pole, even though the initial wave breaking was $\sim$10 hPa.

Overall, the vertical flux of wave activity at the tropopause ($\sim$100 hPa) occurred mainly in the Pacific hemisphere, though at high latitudes (65°–85°N) the 6 January upper tropospheric ridge near 0°E may have aided in splitting the polar vortex.

Preconditioning of the polar vortex by wave 1 was found to be significant in the climatological study of Charlton and Polvani (2007) and the early flux of vertical wave activity on 23 December may have led to preconditioning of the polar vortex, in the sense that, while the 10 hPa 60°N vortex (Fig. 1) was only slightly weaker just before the SSW than earlier times, the polar vortex was displaced off the pole on 28 December (Fig. 3a) enabling the poleward advection of low EPV values. This process is somewhat similar to the advection of low EPV during the January 2006 SSW, where, prior to the January 2006 SSW, the polar vortex was very weak and displaced well off the pole (Coy et al. 2009). In contrast to the strong wave 2 100 hPa upward wave activity flux seen in the January 2009 major SSW (Harada et al. 2010), the SSW of January 2013 was forced mainly in the Pacific hemisphere with high latitude forcing occurring in the Atlantic hemisphere only in the latter stages of the SSW.

The surface low pressure system that rapidly developed under the stratospheric polar vortex on 29 December 2012 was accompanied by a large disturbance in the 360 K potential temperature surface. This storm system produced a strong increase in upward wave activity flux as it developed and propagated under the strong vortex winds (Fig. 15). In the January 2003 and 2006 such strong upper tropospheric development over the North Atlantic also occurred prior to the SSW events (Coy et al. 2009). While not directly associated with persistent large vertical wave activity flux, the North Atlantic storm of 29 December 2012 may have played a role in perturbing the wave structures that led to the SSW. Also the stratospheric vortex may have aided the storm development by providing a strong upper air potential temperature gradient.

The GEOS-5 5-day forecasts accurately predicted the major SSW of January 2013 (Figs. 1 and 2) as well as the upper tropospheric disturbances responsible for the warming (see, for example, Fig. 9). As shown by Dörnbrack et al. (2012) in an analysis of ECMWF, (European Centre of Medium Range Weather Forecasts) products, high resolution and ensemble forecast skill during the major SSW of 2010, forecasting middle stratosphere dynamics is most challenging after the SSW, a time when horizontal EPV gradients are small. In spite of an increased spread seen in the ensemble system, Dörnbrack et al. (2012) showed that the high resolution 5-day ECMWF forecast accurately captured the evolution of the complete 2010 SSW, including the time after the warming. Similarly, the GEOS-5 5-day forecasts at 10 hPa (Fig. 1) are capable of representing the post-SSW dynamics of the lower stratosphere.

In summary, GEOS-5 analyses showed that the SSW of January 2013 was a major warming by 12 UTC 6 January, with a wave-2 vortex splitting pattern. Earlier upward wave activity flux from the upper troposphere ($\sim$23 December 2013) acted to precondition the stratospheric circulation by displacing the $\sim$10 hPa polar vortex off the pole in a wave-1 pattern, enabling the poleward advection of sub-tropical values of EPV into a developing anticyclonic circulation region. This wave breaking reveals itself as an increase in the upward propagating wave activity flux $\sim$3 January, mainly in the Pacific hemisphere. While the polar vortex subsequently split (wave 2 pattern) the wave 2 forcing (upward EP flux) was seen to be smaller than what was found in recent wave 2 SSW events implying an increased role for localized regions (projecting more strongly onto wave 1) of upper tropospheric forcing. Our results show that the SSW began at middle latitudes at $\sim$10 hPa, developing poleward and upward in amplitude before descending over the polar region. Wave breaking that was initially limited in vertical extent was also seen in the January 2006 major SSW (Coy et al. 2009). The dependence of the initial wave breaking altitude on the tropospheric wave forcing remains to be investigated in more detail. The overall success of the 5-day forecasts provides motivation to produce regular 10-day forecasts with GEOS-5, to better support studies of stratosphere-troposphere interaction.

Acknowledgments.

Resources supporting this work were provided by the NASA High-End Computing (HEC) Program through the NASA Center for Climate Simulation (NCCS) at Goddard Space Flight Center. This work was supported by the NASA Modeling, Analysis and Prediction (MAP) program.

REFERENCES

Andrews, D. G., J. R. Holton, and C. B. Leovy, 1987: *Middle Atmosphere Dynamics*. Academic Press, 489 pp.

Baldwin, M. P. and T. J. Dunkerton, 2001: Stratospheric harbingers of anomalous weather regimes. *Science*, **244**, 581–584.

Bloom, S., L. Takacs, A. DaSilva, and D. Ledvina, 1996: Data assimilation using incremental analysis updates. *Mon. Wea. Rev.*, **124**, 1256–1271.

Charlton, A. J. and L. M. Polvani, 2007: A new look at stratospheric sudden warmings. Part I: Climatology and modeling benchmarks. *J. Climate*, **20**, 449–469.

Chou, M.-D. and M. J. Suarez, 1999: A solar radiation parameterization for atmospheric studies. NASA Tech. Rep. Series on Global Modeling and Data Assimilation NASA/TM-1999-104606, NASA, 40 pp.

Chou, M.-D., M. J. Suarez, X. Z. Liang, and M. M.-H. Yan, 2001: A thermal infrared radiation parametrization for atmospheric studies. NASA Tech. Rep. Series on Global Modeling and Data Assimilation NASA/TM-2001-104606, NASA, 56 pp.

Coy, L., S. D. Eckermann, and K. Hoppel, 2009: Planetary wave breaking and tropospheric forcing as seen in the stratospheric sudden warming of 2006. *J. Atmos. Sci.*, **66**, 495–507, doi:10.1175/2008JAS2784.1.

Coy, L., S. D. Eckermann, K. W. Hoppel, and F. Sassi, 2011: Mesospheric precursors to the major stratospheric sudden warming of 2009: Validation and dynamical attribution using a ground-to-edge-of-space data assimilation system. *J. Adv. Model. Earth Syst.*, **3**, M10002, doi:10.1029/2011MS000067.

Dörnbrack, A., M. C. Pitts, L. R. Poole, Y. J. Orsolini, K. Nishii, and H. Nakamura, 2012: The 2009–2010 arctic stratospheric winter — general evolution, mountain waves and predictability of an operational weather forecast model. *Atmos. Chem. Phys.*, **12**, 3659–3675, doi:10.5194/acp-12-3659-2012.

Garcia, R. R. and B. A. Boville, 1994: Downward control of the mean meridional circulation and temperature distribution of the polar winter stratosphere. *J. Atmos. Sci.*, **51**, 2238–2245.

Gelaro, R., R. H. Langland, S. Pellerin, and R. Todling, 2010: The THORPEX observation impact intercomparison experiment. *Mon. Wea. Rev.*, **138**, 4009–4025.

Harada, Y., G. Atsushi, H. Hiroshi, and N. Fujikawa, 2010: A major stratospheric sudden warming event in January 2009. *J. Atmos. Sci.*, **67**, 2052–2069.

Harvey, V. L. and M. H. Hitchman, 1996: A climatology of the Aleutian high. *J. Atmos. Sci.*, **53**, 2129–2143.

Hoppel, K. W., N. L. Baker, L. Coy, S. D. Eckermann, J. P. McCormack, G. E. Nedoluha, and D. E. Siskind, 2008: Assimilation of stratospheric and mesospheric temperatures from MLS and SABER in a global NWP model. *Atmos. Chem. Phys.*, **8**, 6103–6111, doi:10.5194/acp-8-6103-2008.

Kodera, K., H. Mukougawa, and A. Fujii, 2013: Influence of the vertical and zonal propagation of stratospheric planetary waves on tropospheric blockings. *J. Geophys. Res. Atmos.*, **118**, 8333–8345, doi:10.1002/jgrd.50650.

Kuttippurath, J. and G. Nikulin, 2012: A comparative study of the major sudden stratospheric warnings in the Arctic winters 2003/2004–2009/2010. *Atmos. Chem. Phys.*, **12**, 8115–8129, doi:10.5194/acp-12-8115-2012.

Limpasuvan, V., D. W. J. Thompson, and D. L. Hartmann, 2004: The life cycle of the Nnorthern Hemisphere sudden stratospheric warnings. *J. Climate*, **17**, 2584–2596.

Lin, S.-J., 2004: A vertically Lagrangian finite-volume dynamical core for global models. *Mon. Wea. Rev.*, **132**, 2293–2307.

Matsuno, T., 1971: A dynamical model of the stratospheric sudden warming. *J. Atmos. Sci.*, **28**, 1479–1494.

McFarlane, N. A., 1987: The effect of orographically excited gravity wave drag on the general circulation of the lower stratosphere and troposphere. *J. Atmos. Sci.*, **44**, 1775–1800.

McIntyre, M. E. and T. N. Palmer, 1983: Breaking planetary waves in the stratosphere. *Nature*, **305**, 593–600.

Molod, A., L. Takacs, M. Suarez, J. Bacmeister, I.-S. Song, and A. Eichmann, 2012: The GEOS-5 Atmospheric General Circulation Model: Mean Climate and Development from MERRA to Fortuna. NASA Tech. Rep. Series on Global Modeling and Data Assimilation, NASA/TM-2012-104606, Vol. 28, NASA, 117 pp.

Pawson, S., et al., 2007: Stratospheric transport using 6-h-averaged winds from a data assimilation system. *J. Geophys. Res.*, **112**, D23103, doi:10.1029/2006JD007673.

Plumb, R. A., 1985: On the three-dimensional propagation of stationary waves. *J. Atmos. Sci.*, **42**, 217–229.

Purser, R. J., W.-S. Wu, D. F. Parrish, and N. M. Roberts, 2003a: Numerical aspects of the application of recursive filters to variational statistical analysis. Part I: Spatially homogeneous and isotropic Gaussian covariances. *Mon. Wea. Rev.*, **131**, 1524–1535.

Purser, R. J., W.-S. Wu, D. F. Parrish, and N. M. Roberts, 2003b: Numerical aspects of the application of recursive filters to variational statistical analysis. Part II: Spatially inhomogeneous and anisotropic general covariances. *Mon. Wea. Rev.*, **131**, 1536–1548.

Rienecker, M. M., et al., 2008: The GEOS-5 Data Assimilation System - Documentation of Versions 5.0.1, 5.1.0, and 5.2.0. NASA Tech. Rep. Series on Global Modeling and Data Assimilation, NASA/TM-2008-104606, Vol. 27, NASA, 118 pp.

Rienecker, M. M., et al., 2011: MERRA: NASA's Modern-Era Retrospective Analysis for Research and Applications. *J. Climate*, **24**, 3624–3648, doi:http://dx.doi.org/10.1175/JCLI-D-11-00015.1.

Sanders, F. and J. R. Gyakum, 1980: Synoptic-dynamic climatology of the "bomb". *Mon. Wea. Rev.*, **108**, 1589–1606.

Sjoberg, J. P. and T. Birner, 2012: Transient tropospheric forcing of sudden stratospheric warnings. *J. Atmos. Sci.*, **69**, 3420–3432.

Wu, W.-S., R. J. Purser, and D. F. Parrish, 2002: Three-dimensional variational analysis with spatially inhomogeneous covariances. *Mon. Wea. Rev.*, **130**, 2905–2916.

List of Figures

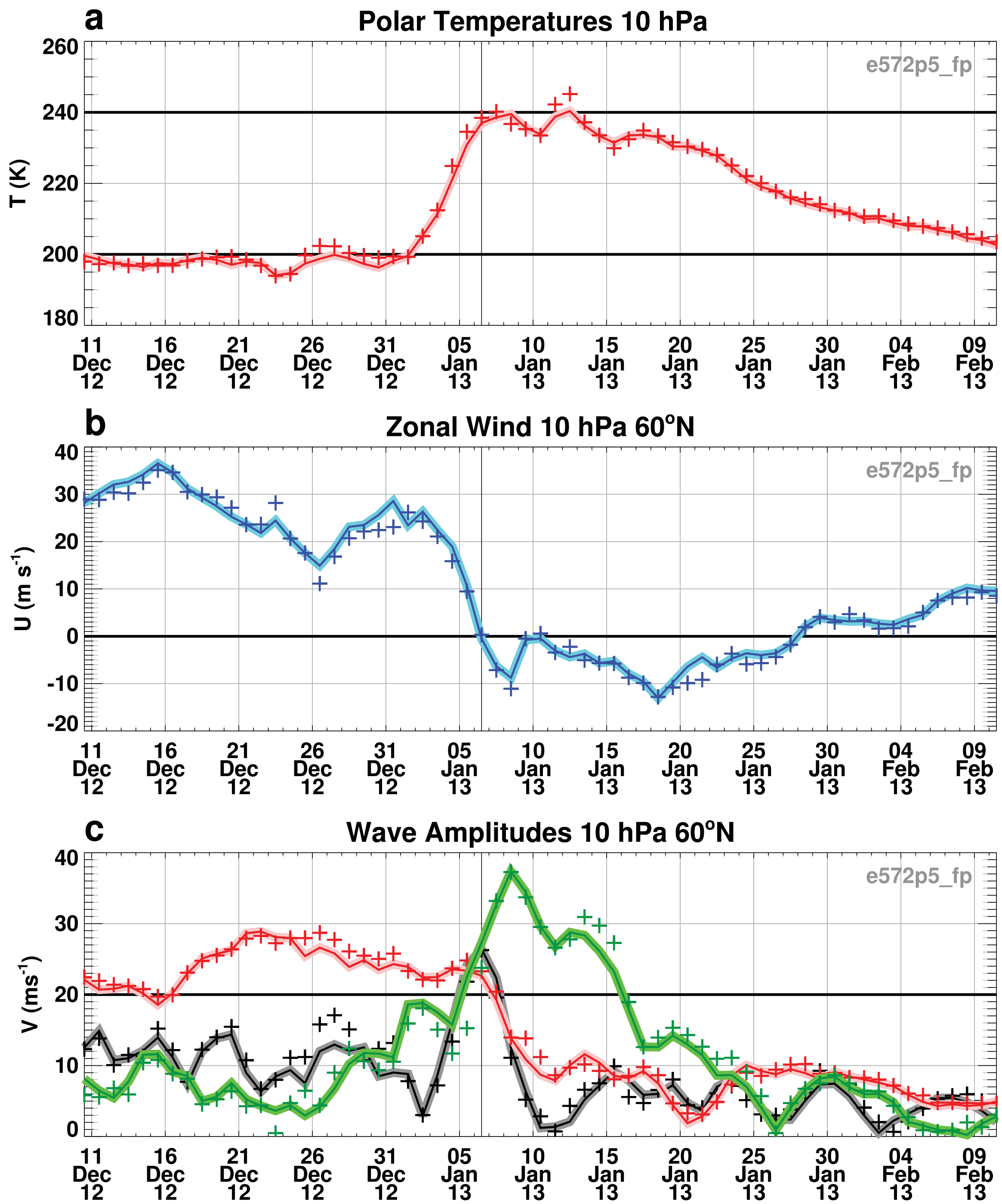

FIG. 1. Daily (12 UTC) values showing the 10 hPa evolution for a) North Pole temperature (K), b) 60°N zonal averaged zonal wind (ms^{-1}), and c) 60°N meridional wind amplitudes (ms^{-1}) for zonal wave numbers 1 (red), 2 (green), and 3 (black). The sold lines are based on the analyses. The plus symbols denote the corresponding 5-day forecasted values. The heavy vertical line denotes 6 January 2013, the SSW date.

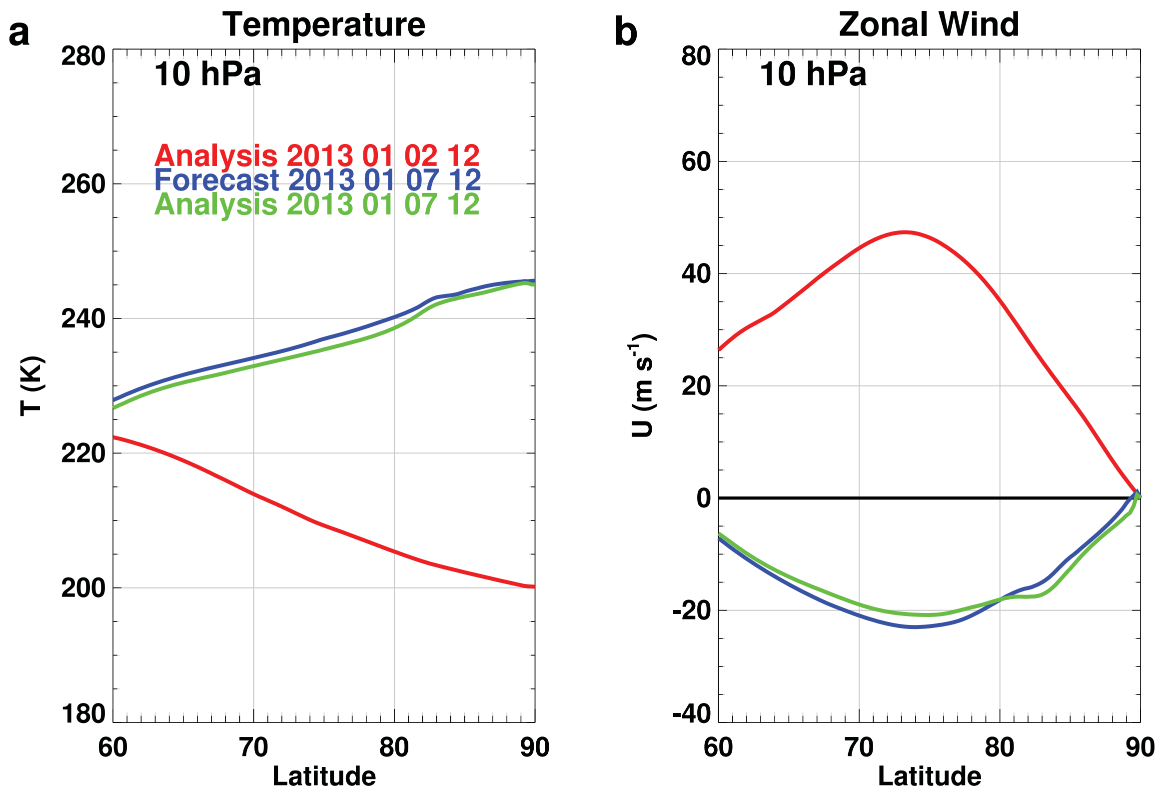

FIG. 2. Zonal mean a) temperature (K) and b) zonal wind (ms^{-1}) at 10 hPa as a function of latitude for the five day forecast (blue curves) and analysis (green curves) from the 2 January 2013 12UTC initial time analysis (red curves).

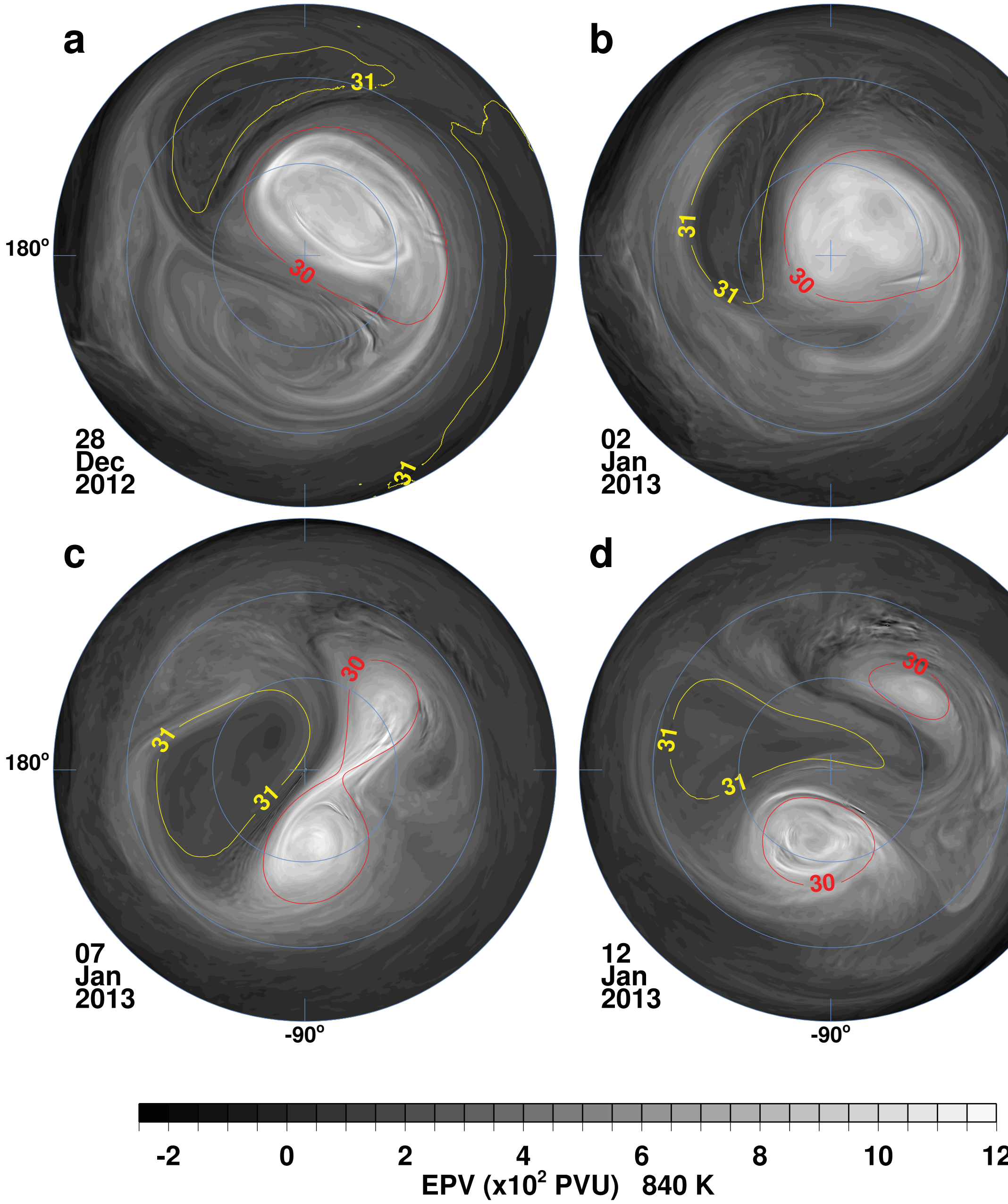

FIG. 3. EPV (x10^2 PVU, gray shading) on the 840 K potential temperature surface for a) 28 Dec 2012, b) 2 Jan 2013, c) 7 Jan 2013, and d) 12 Jan 2013. Also plotted are the 30.25 km and 31.25 km (red and yellow respectively) 10 hPa geopotential height contours. The polar Lambert projection of the northern hemisphere has 90°W at the bottom with blue circles at 30°N and 60°N.

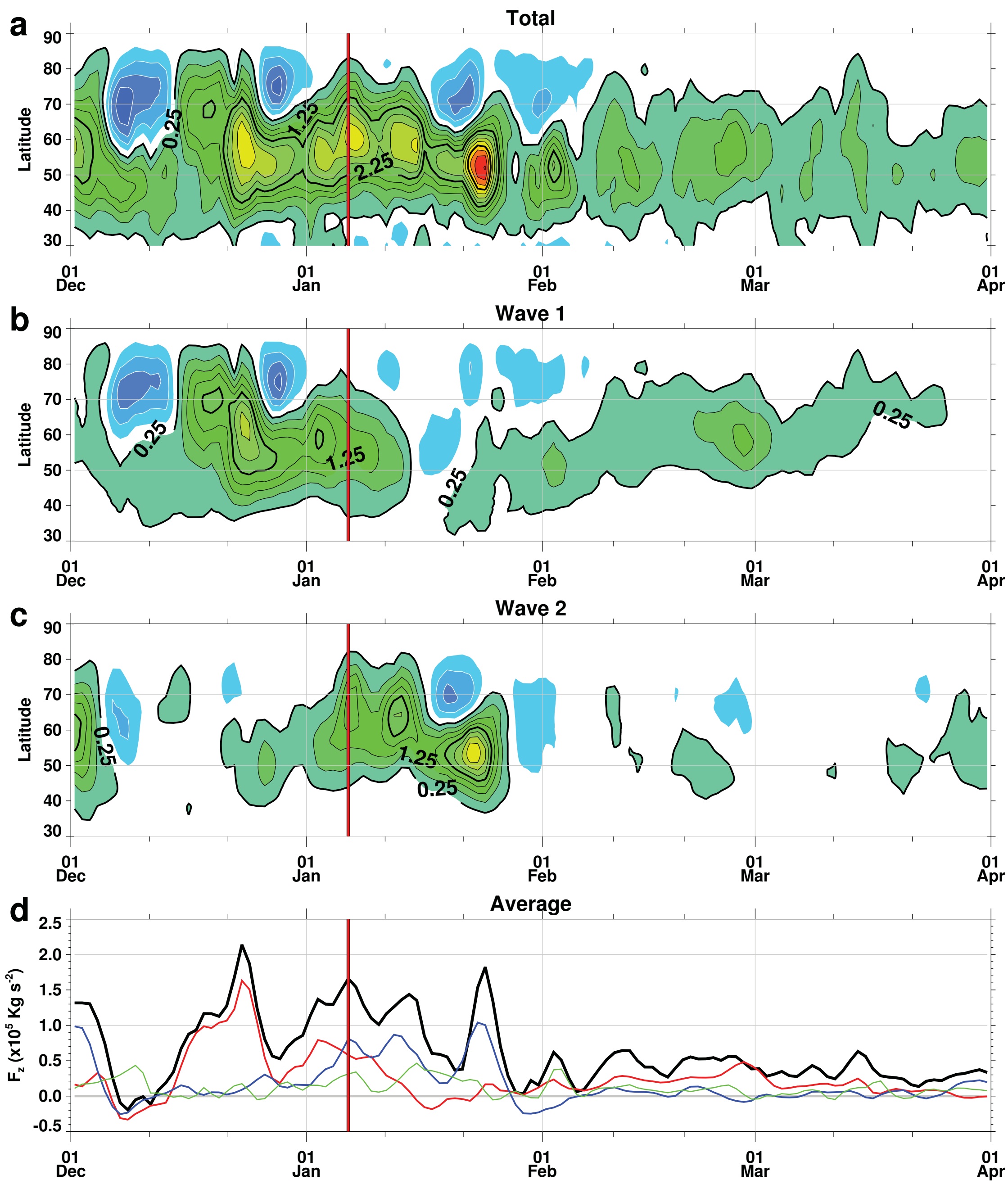

FIG. 4. Vertical EP flux at 100 hPa for a) all waves, b) wave 1, and c) wave 2 as a function of latitude and time with a contour interval of 0.5×10^5 Kg s^{-2} and d) the latitudinal average of all waves (black), wave 1 (red), wave 2 (blue), and wave 3 (green).

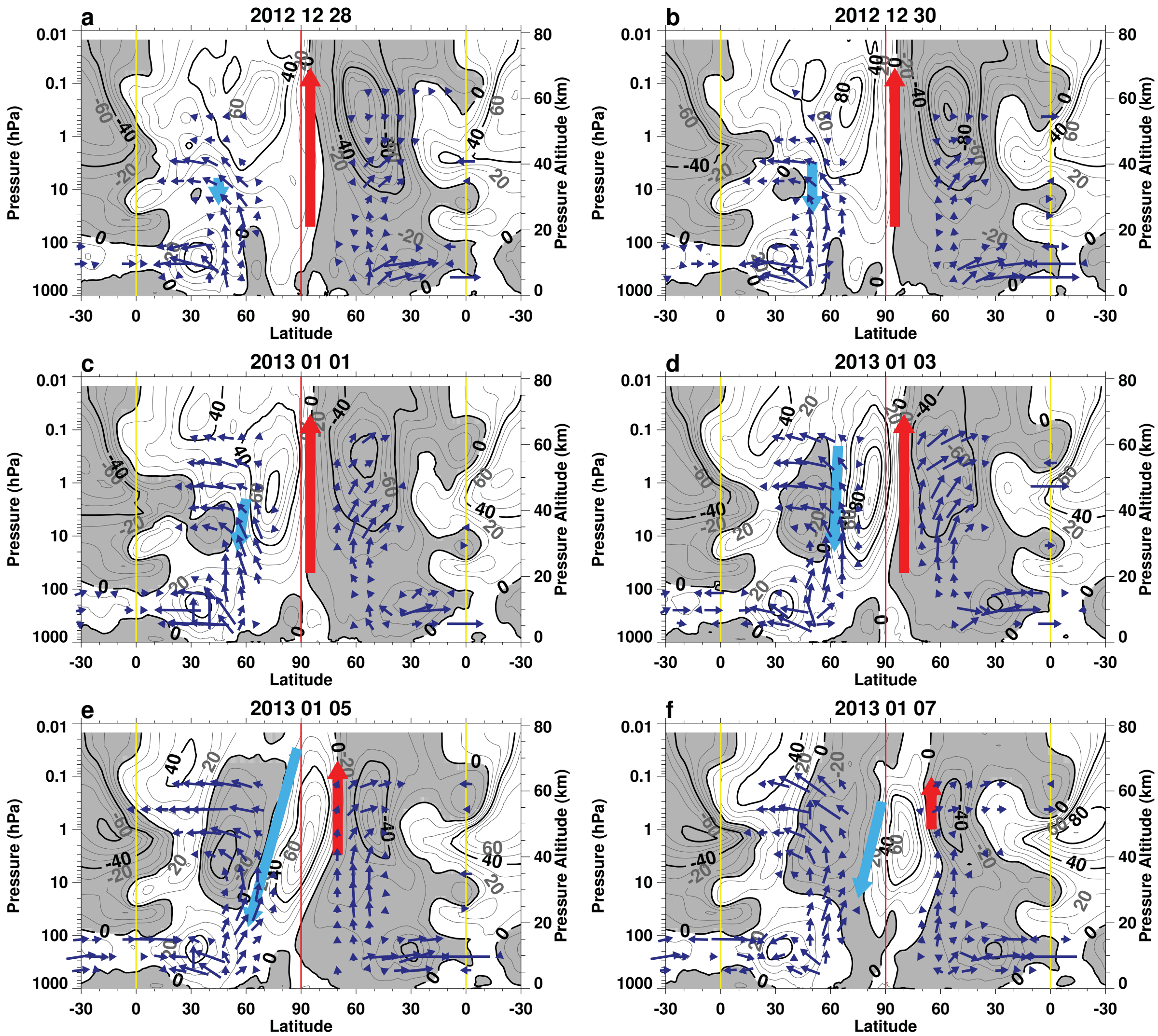

FIG. 5. Contour plots of zonal wind (ms^{-1}) as a function of latitude (degrees) and pressure (hPa) at two-day intervals: a) 28 Dec 2012, b) 30 Dec 2012, c) 1 Jan 2013, d) 3 Jan 2013, e) 5 Jan 2013 and f) 7 Jan 2013, all at 12 UTC. The zonal winds are hemispheric averages over longitude with the left (right) half of each panel centered on 180°E (0°E). Shading denotes winds that are into the page. Dark blue arrows denote the hemispheric averaged wave activity flux vectors, scaled at each pressure by the maximum vertical component over December 2012 to January 2013. Large arrows denote axis of positive (Red) and negative (light blue) relative vorticity.

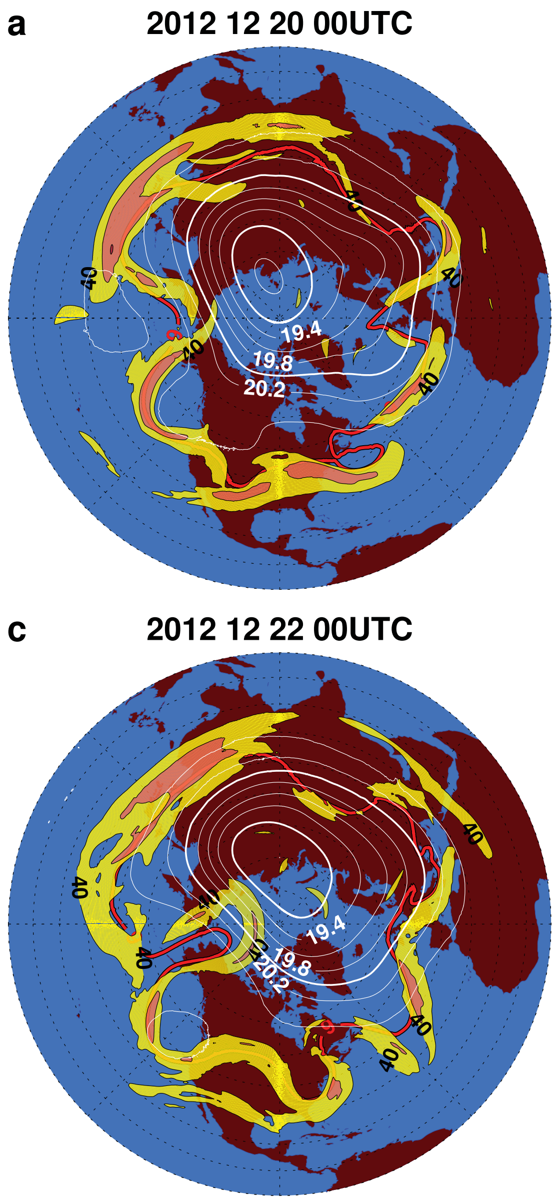

FIG. 6. Wind speed at 300 hPa (contoured at 40, 60, and 80 ms^{-1}; yellow, brown, and red filled contours respectively) and geopotential heights at 50 hPa (contour interval of 0.2 km, white contours) for a) 20, b) 21, c) 22, and d) 23 December 2012 at 00 UTC. The thick red curve denotes the 9 km geopotential height contour at 300 hPa.

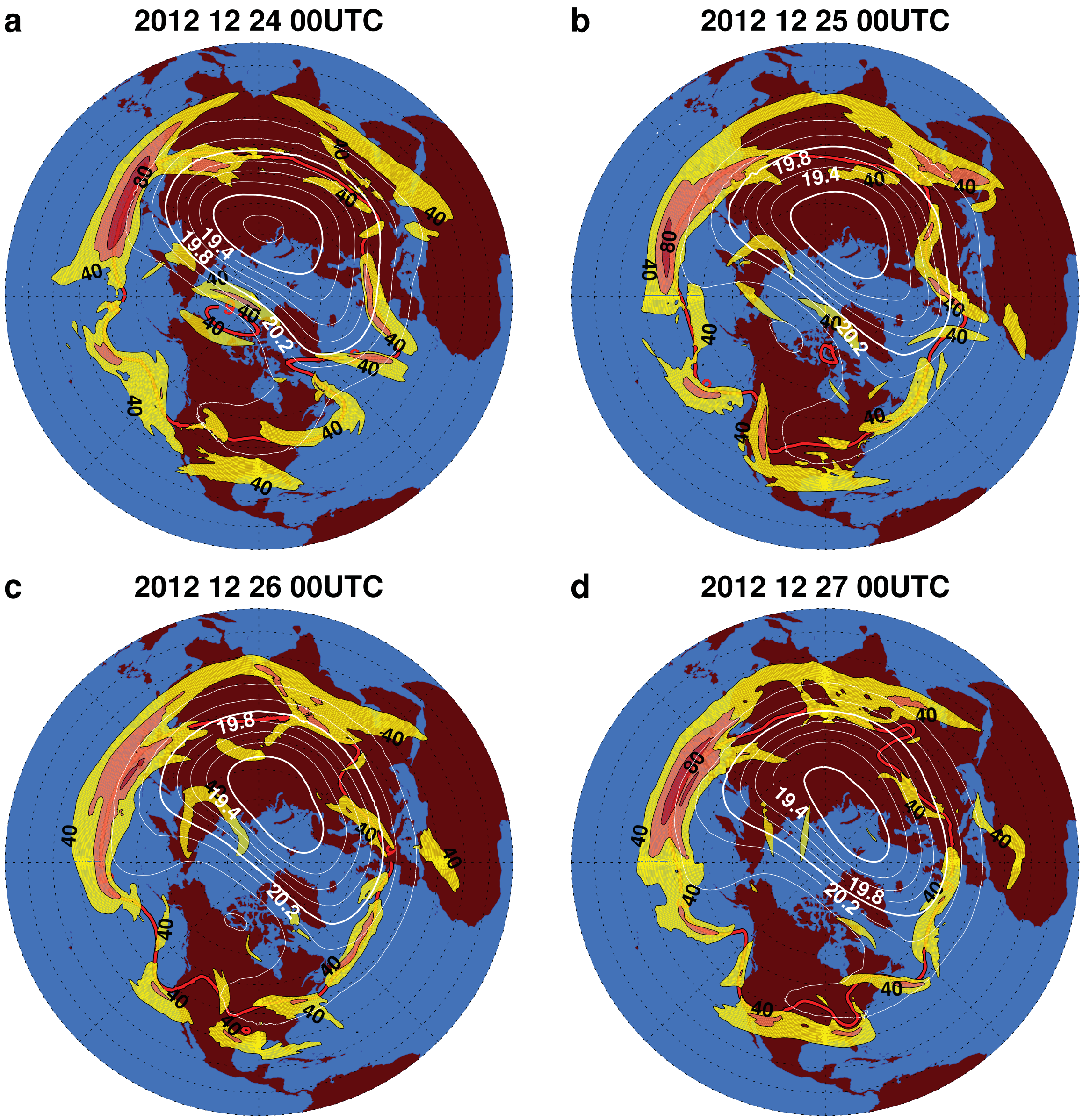

Fig. 7. As in Fig. 6 for a) 24, b) 25, c) 26, and d) 27 December 2012 at 00 UTC.

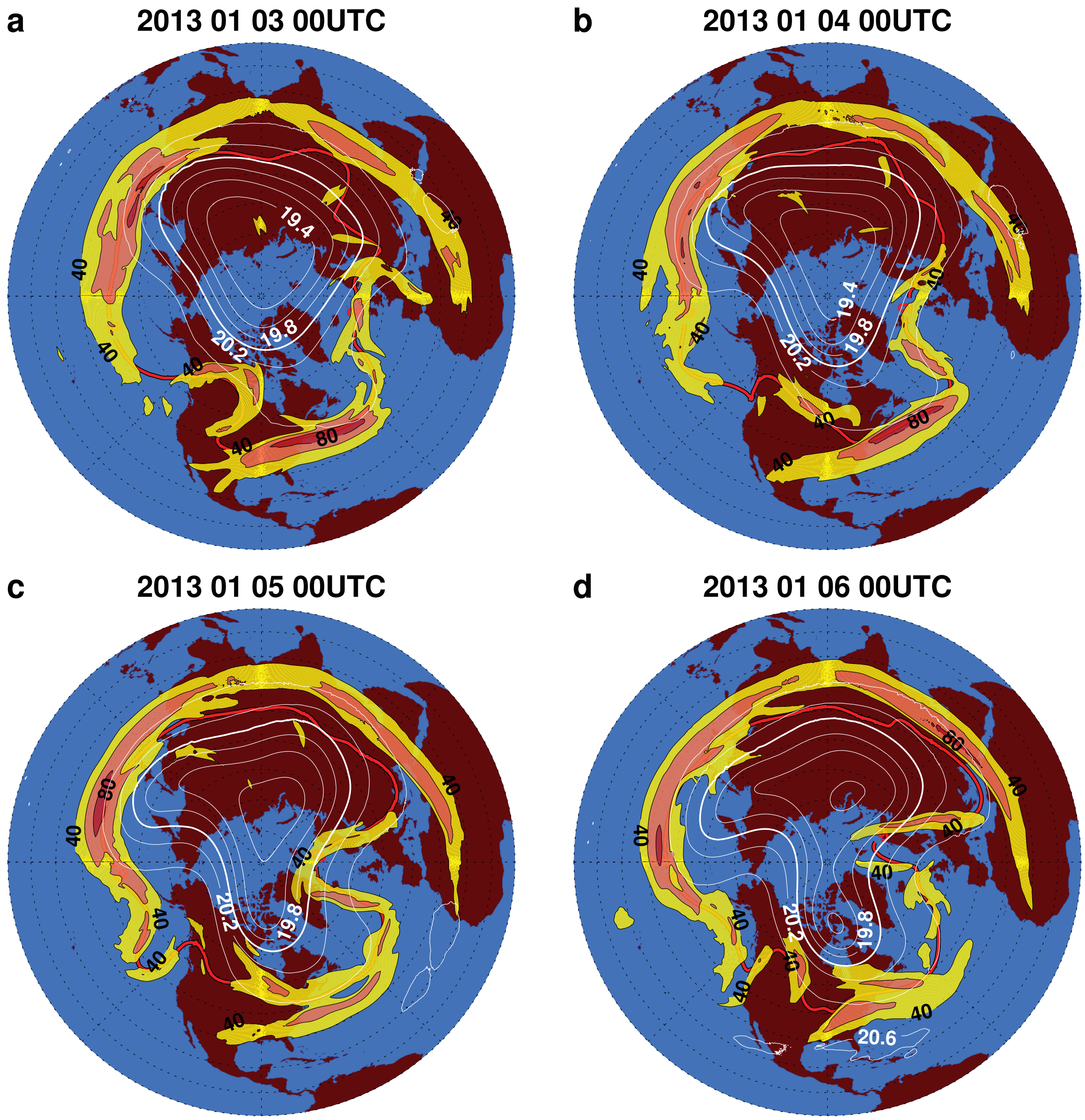

FIG. 8. As in Fig. 6 for a) 3, b) 24 c) 5, and d) 6 January 2013 at 00 UTC.

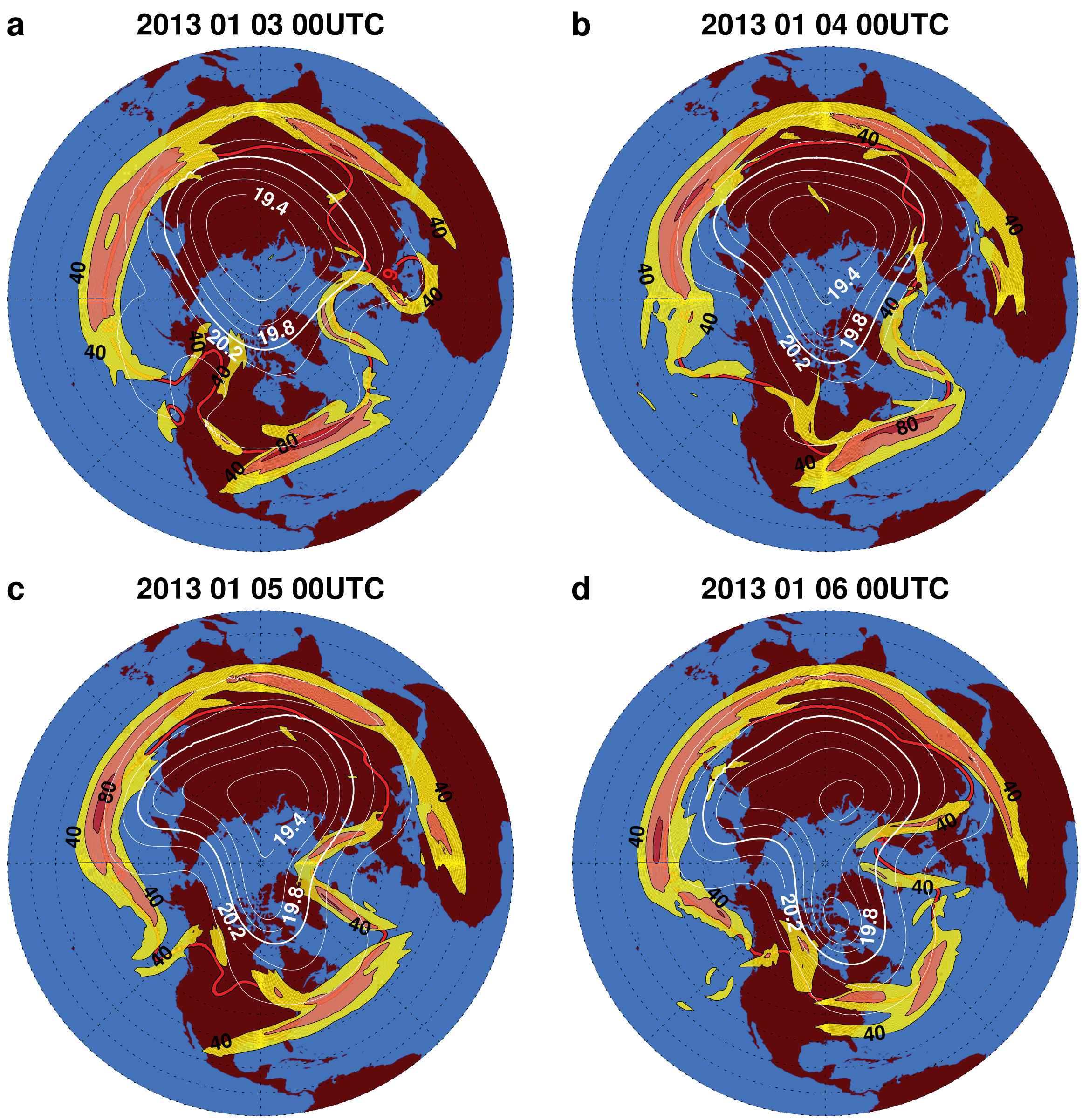

FIG. 9. Five day forecasts plotted as in Fig. 6 for a) 3, b) 4 c) 5, and d) 6 January 2013 at 00 UTC.

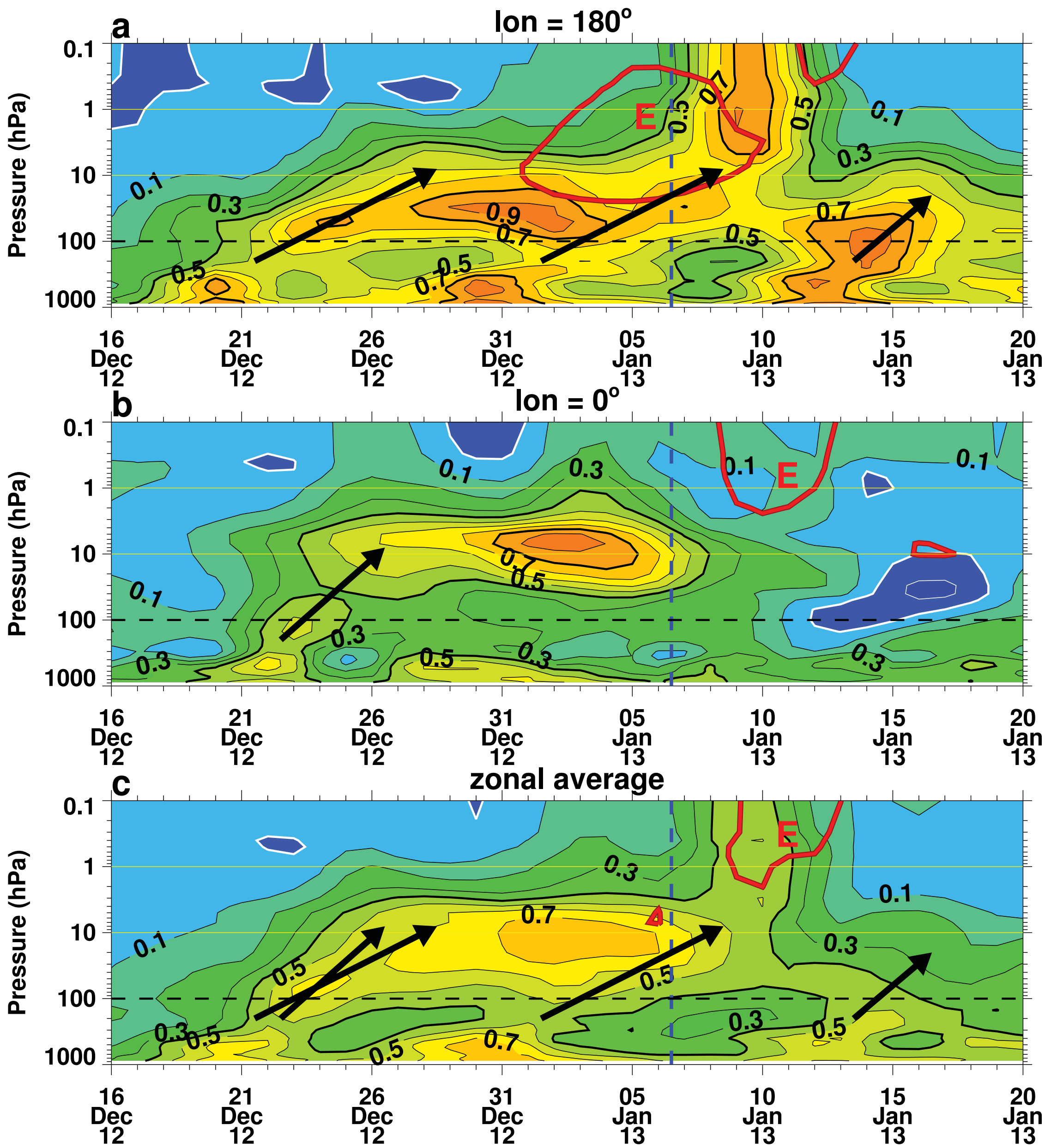

FIG. 10. Time altitude contour plot of the vertically-scaled, vertical component of the wave activity flux ($\times 10^{-4} p^{-1}$, black contours) and zero zonal wind contour (red) averaged over latitudes 30°–60°N and a) the hemisphere centered on 180°E, b) the hemisphere centered on 0°E, c) zonally averaged. The black arrows suggest times of vertical wave propagation.

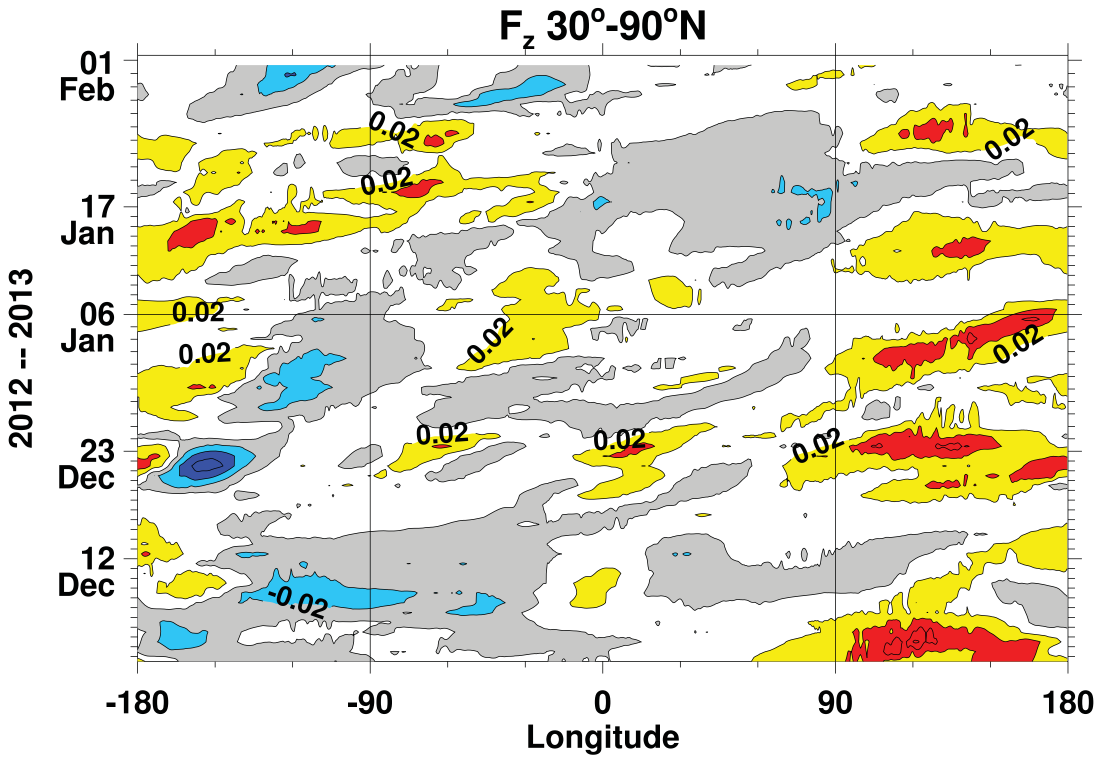

FIG. 11. Vertical wave activity flux at 100 hPa averaged over 30°–90°N as a function of longitude and time. Contour interval of 0.02 $m^2\ s^{-2}$.

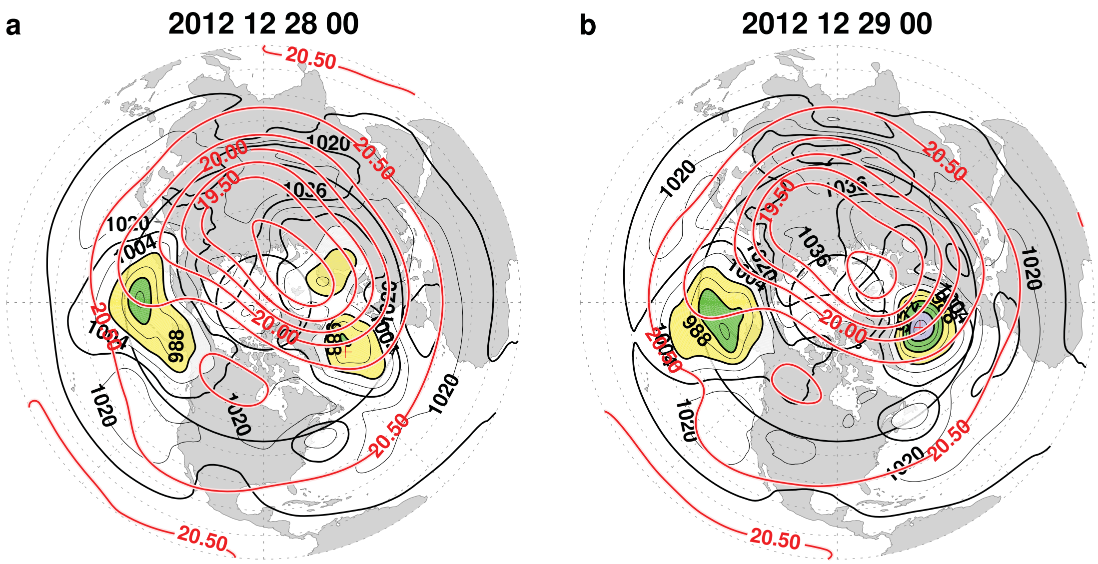

FIG. 12. Sea level pressure (black contours, contour interval: 16 hPa) for a) 28 and b) 29 December 2012 at 00 UTC. Also plotted are the corresponding 50 hPa geopotential heights (red curves labeled in km).

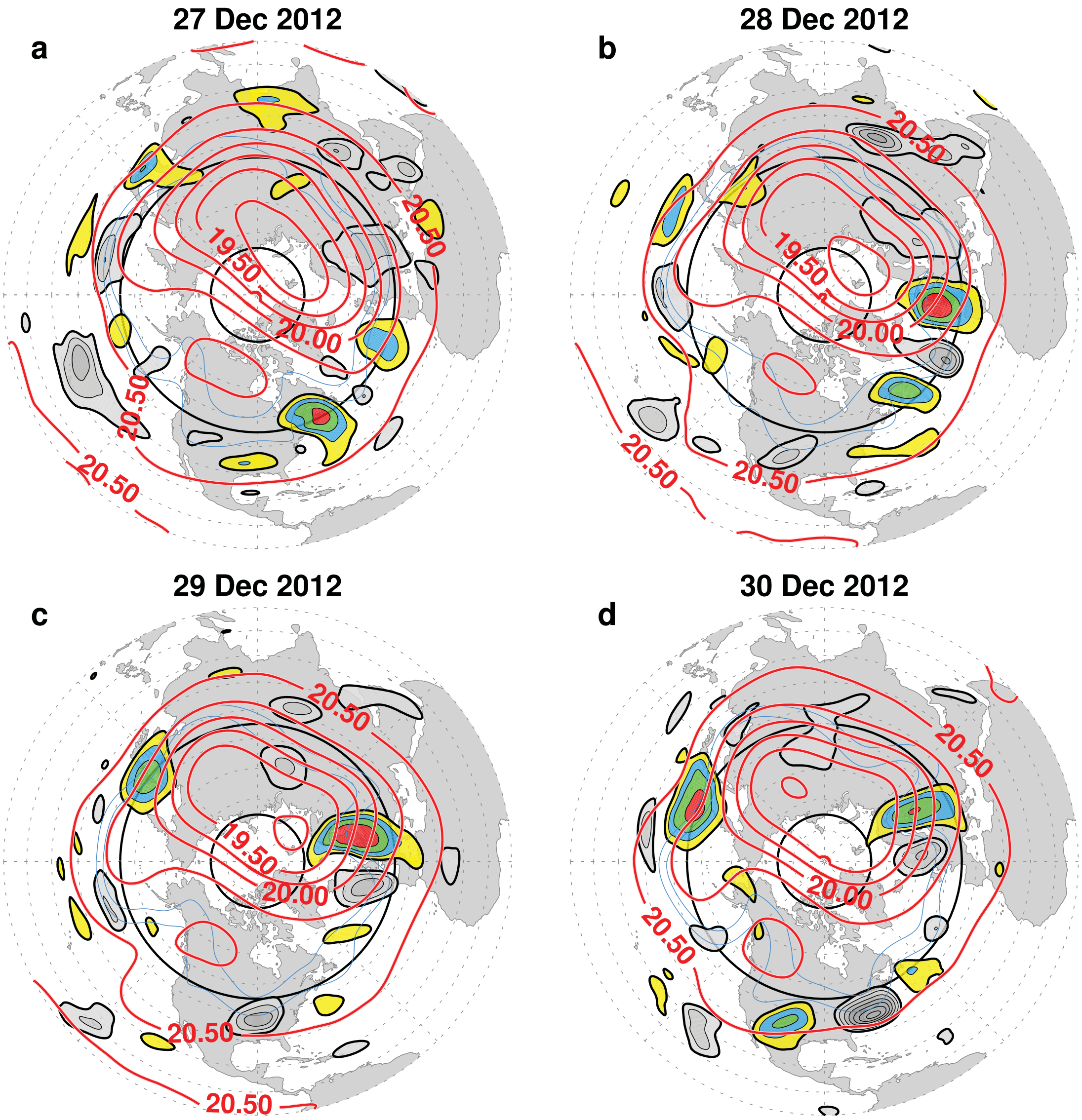

Fig. 13. Polar plots of 360 K potential temperature surface height perturbations with respect to a 7 day running average (contour intervals of 0.25 km starting from ±0.5 km, colors are positive; grays are negative), 50 hPa geopotential heights (red contours, labeled in km), and 200 hPa heights (blue curves) at 11.25 and 11.5 km for a) 27, b) 28, c) 29, and d) 30 December 2012.

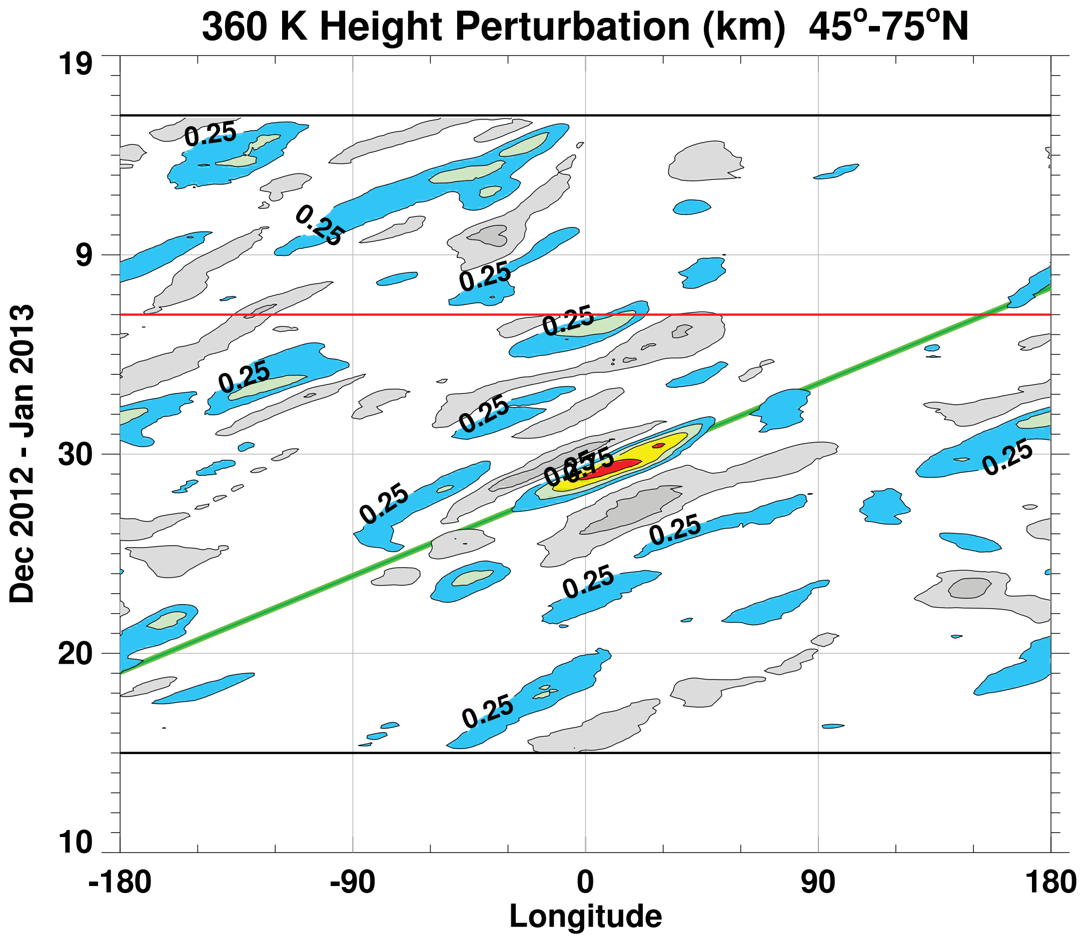

FIG. 14. Time longitude plot of the 360 K potential temperature surface height perturbations with respect to a running 7 day mean, averaged over 45°–75°N. The contour interval is 0.25 km, color (gray) shaded contour interval are positive (negative), and the zero contour is not plotted. For reference, the green line has a slope of 12 ms^{-1}.

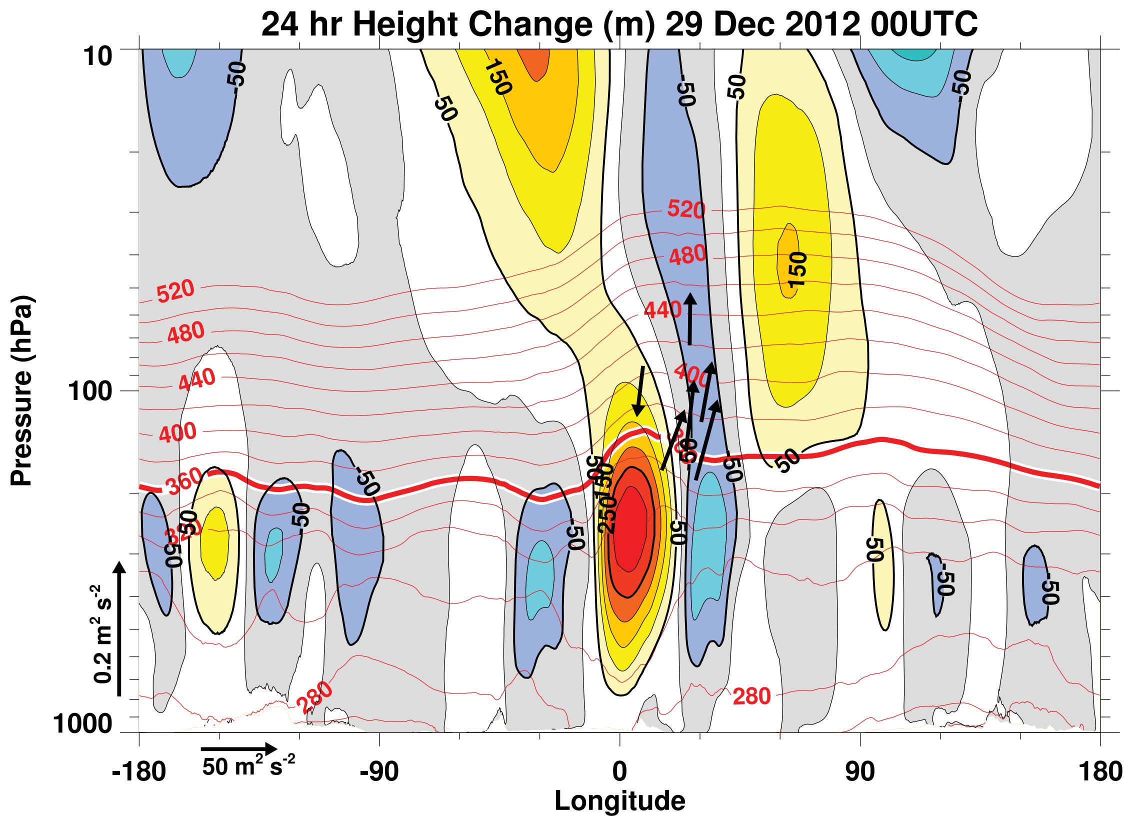

Fig. 15. Longitude height cross section at 57–63N of the 24 change in geopotential height (m) ending on 29 December 2012 00 UTC (color filled contours, contour interval: 50 m). Also plotted is potential temperature (red contours, contour interval: 20 K). The 360 K contour is highlighted in bold red. The arrows (plotted above 150 hPa) depict the 24 hr change in the wave activity flux.

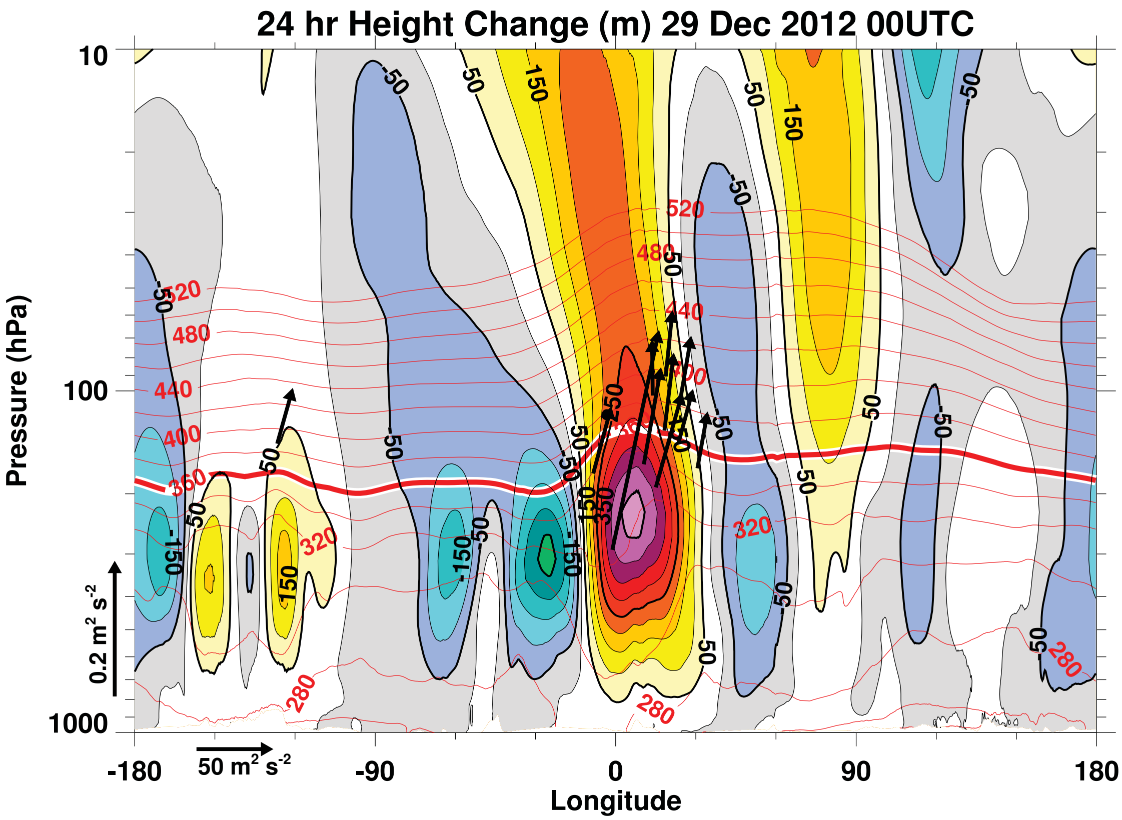

FIG. 16. Same as Fig. 15 but for a 5-day forecast ending on 29 December 2013 00 UTC.

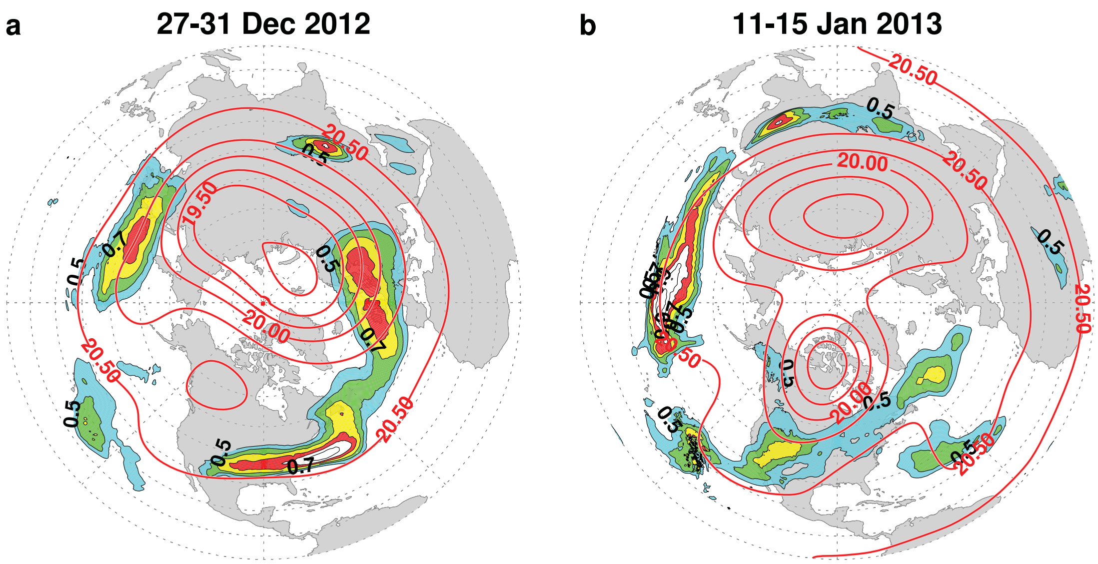

FIG. 17. Standard deviation of the 360 K potential temperature surface perturbations (0.25 km contour interval, lowest contour of 0.5 km) with respect to the time periods: a) 27–3 December 2012, and b) 11–15 January 2013. Also plotted are the 50 hPa geopotential heights (red curves labeled in km) averaged over the same time periods.